night from 18.00 to 6.30 h are presented in figure 1. In animals allowed free access to food, intestinal calcium transport exhibited rhythmic changes, being low in the morning and high at night. At 10.00 h active calcium transport was lowest and limited to duodenum only (segment No. 1). The increase in duodenal transport activity occurring at evening and at night was accompanied by a gradual appearance and enhancement of active calcium transport in the contiguous part of the small intestine (segments Nos 2 and 3). The highest transport was achieved at 22.00 h, 4 h after darkness began. Restricted feeding of rats during the daytime from 9.00 to 15.00 h resulted in phase shift of diurnal periodicity of intestinal calcium transport (figure 1, b). The highest transport occurred in the morning during the time of food presentation. At 22.00 h the transport was low and limited to duodenum only. Phase shifting of diurnal rhythm of active calcium transport in the intestine could have been achieved also by the changes in the light-dark cycle. In rats maintained in reversed light-dark schedules (12:12) with free access to food, the transport was always low during light period and high in dark period with a peak 3 h after the start of darkness (figure 2).

The results presented indicate that both light-dark transition and the time of food presentation do play a role as 'Zeitgeber' in determining the phase of daily rhythm of active calcium transport in rat intestine. The time of food intake, however, appears to be a more potent synchronizer than the light-dark cycle. This assumption is supported by the experiments with feeding restricted to light phase (figure 1). On the other hand, even in rats fasted for 48 h, an increase of active calcium transport did occur from 170 ± 18 at 10.00 h to 283 ± 18 nmoles · 90 min^{-1} at 22.00 h in the duodenum; in the intestinal segments Nos 2 and 3 from fasted rats, there was no active calcium transport at 10.00 h whereas at 22.00 h the transport was 83 ± 15 and 40 ± 8, respectively. Thus it appears likely that, although cyclic food intake may be a prerequisite for diurnal changes in intestinal calcium transport, the rise in transport activity is not a simple, direct consequence of food digestion only.

Further studies are needed to elucidate the exact mechanism of the daily rhythm of active calcium transport in rat intestine and its physiological significance. It is of interest to note, however, that the sequential pattern of rhythmic increase of calcium transport along the proximal region of small intestine is inversely correlated with diurnal fluctuations of plasma calcium concentration[3,4] and follows a general time-dependent sequence of adaptive response in active transport ability along intestinal length during pregnancy, lactation and dietary calcium restriction[6,8].

1 This work has been supported by Polish Academy of Sciences within the project MR II.1.1.6.
2 E. Bunning, in: The physiological clock. Springer Verlag, New York 1973.
3 A.M. Perault-Staub, J.F. Staub and G. Milhaud, Endocrinology *95*, 480 (1974).
4 R.V. Talmage, J.H. Roycroft and J.J.B. Anderson, Calcif. Tissue Res. *17*, 91 (1975).
5 W. Jubiz, J.M. Canterbury, E. Reiss and F. Tyler, J. clin. Invest. *51*, 2040 (1972).
6 L. Michalska, J. Wróbel and M. Szczepańska-Konkel, Acta biochim. pol. *23*, 109 (1976).
7 J. Wróbel, L. Michalska and R. Niemiro, FEBS Lett. *29*, 121 (1973).
8 J. Wróbel, L. Michalska and G. Nagel, 16th Meeting Polish Biochem. Soc., abstr., p. 70 (1978).

Lymphocytes, but not cancer cells are able to penetrate into the rat embryo yolk sac wall

P. Sträuli and Marie-Françoise Maignan

Division of Cancer Research, Institute of Pathology, University of Zürich, Birchstrasse 95, CH-8050 Zürich (Switzerland), 9 April 1979

Summary. Normal rat lymphocytes and cells of 2 highly invasive tumors, the L5222 rat leukemia and the V2 rabbit carcinoma, were inoculated in vitro on the mesothelial surface of the visceral wall of the rat embryo yolk sac. After 48 h, lymphocytes, without any damage being inflicted on the mesothelial cells, had penetrated deeply into the yolk sac wall, whereas both kinds of cancer cells had destroyed the mesothelial cells, but not advanced beyond the basal lamina.

It is well established that some classes of normal cells (leukocytes, macrophages) and many cancer cells are able to migrate within the body's extracellular matrix. The mechanism responsible has not been clarified so far. In order to investigate the encounter between cells and extracellular matrix in vitro, we have inoculated normal and neoplastic cells on the visceral wall of the rat embryo yolk sac, which is characterized by a particularly thick layer of collagen-rich material.

Materials and methods. The visceral wall of the rat embryo yolk sac consists mainly of a 7 µm layer of thin, plaited collagen microfibrils embedded into an electronoptically unstructured ground substance. On one side, this layer is covered by mesothelial cells with their basal lamina, on the opposite side by connective tissue and epithelium. Fragments of the whole visceral yolk sac wall were explanted on to a semi-solid mixture of Bacto-Agar and tissue culture medium[1]. The following cells were used for inoculation experiments: Rat lymphocytes obtained by filtration of minced lymph nodes through several layers of gauze; L5222 rat leukemia cells[2] from the peritoneal cavity of BDIX rats; V2 carcinoma cells isolated by trypsinization of 24-h-cultures of cells derived from solid tumors grown in the peritoneal cavity of New Zealand rabbits. The cells were washed in medium, and pellets were deposited on the mesothelial surface of the yolk sac wall explanted 2 h previously. Specimens for transmission electron microscopy were removed 8, 24, 48 and 72 h after inoculation. Up to 48 h neither the yolk sac fragments nor the deposited cells showed any regressive changes. Such alterations, however, were recognizable at 72 h, and exploitation of the model was therefore limited to 48 h.

Results. Ultrathin sections provide evidence for completely different behavior patterns for lymphocytes and cancer cells. In the presence of lymphocytes, the mesothelial cells remain intact throughout the observation period. At 24 h, lymphocytes are either found between mesothelial cells and their basal lamina, or within pouch-like protrusions of the latter extending into the collagen layer (figure 1). Concerning the attainment of the submesothelial position, our data

rather support an intercellular than an intracellular passage. At 48 h, the lymphocyte-containing protrusions of the basal lamina, occasionally lined by cytoplasmic extensions of the mesothelial cells (figure 1), have become elongated and tube-like. However, we have not, so far, observed the expansion of such tubes across the whole width of the collagen layer.

In contrast to lymphocytes, leukemia cells and carcinoma cells cause the disappearance of the mesothelium and, to some extent, of its basal lamina; but the cancer cells do not advance beyond the latter. At 24 h and later, L5222 leukemia cells lie directly upon the basal lamina. Most of the cells have assumed the polarized shape characteristic for cells preparing for, or engaged in, locomotion[3,4] (figure 2). V2 carcinoma cells form an epithelium-like layer completed at 24 h and resting upon a basal lamina with faded structure and multiple small defects. Through these gaps, short projections of the carcinoma cells extend into the collagen layer. In many instances, small portions of collagen are surrounded by converging extensions of the cancer cells (figure 3), but so far, we have no proof for internalization of this material.

Discussion. In their natural host, L5222 leukemia and V2 carcinoma cells are highly invasive. For L5222, locomotion is a major factor of invasion[5], whereas for V2, locomotion, although detectable[6], appears to be less important than proteolytic action[7-9]. While both tumors also give some indication of their prevailing modes of invasion – locomotion and lysis – if explanted on the rat yolk sac wall, they fail to penetrate into the collagen-rich stratum, at least within the available observation period. For lymphocytes, on the other hand, the same period is largely sufficient for infiltrating and, conjecturally, traversing this structure. It

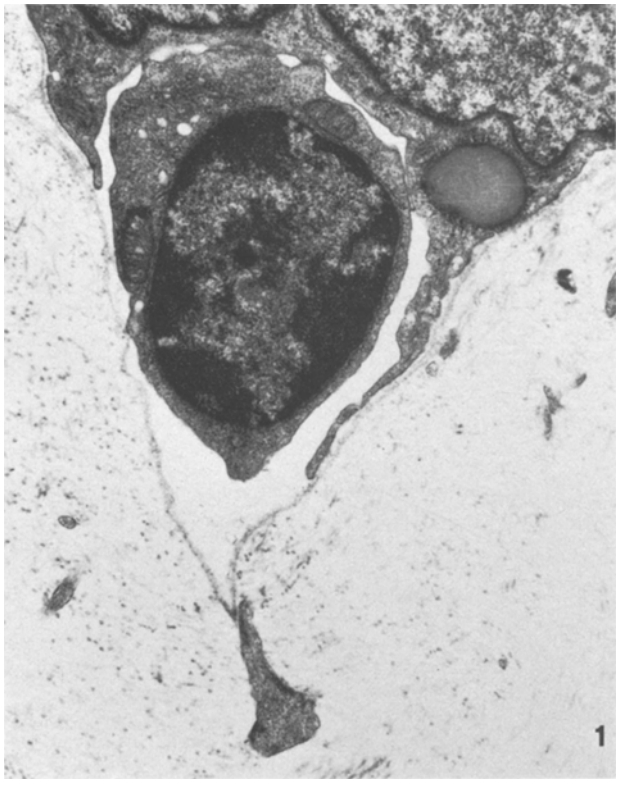

Fig. 1. Lymphocyte within pouch formed by bottom side of mesothelial cell (top) and basal lamina. Note extensions of mesothelial cell along inner surface of pouch. Electrondense structures within extracellular matrix are parts of fibroblasts. 24 h after inoculation. × 13,700.

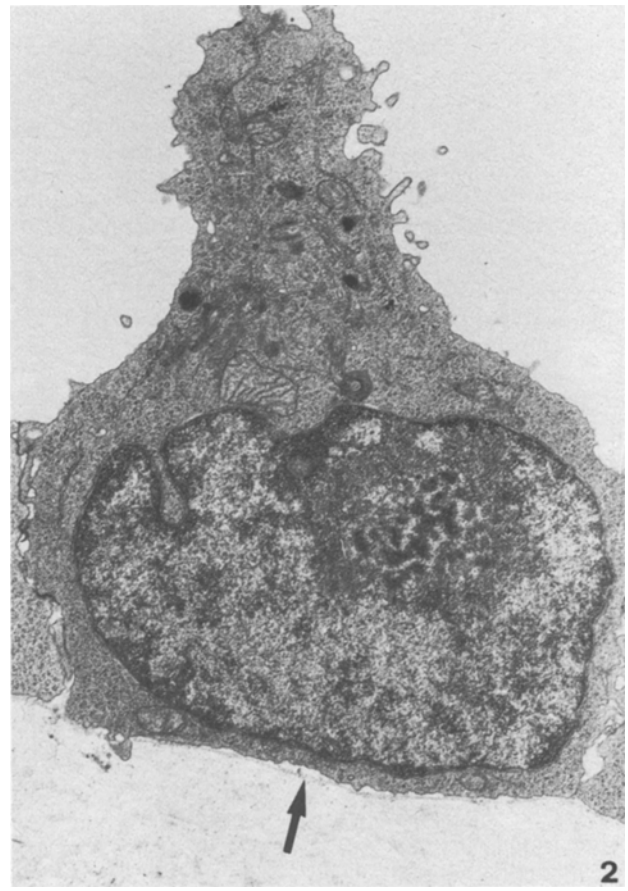

Fig. 2. L5222 leukemia cell in polarized configuration lying upon remains of basal lamina (arrow) of vanished mesothelium. 24 h after inoculation. × 7400.

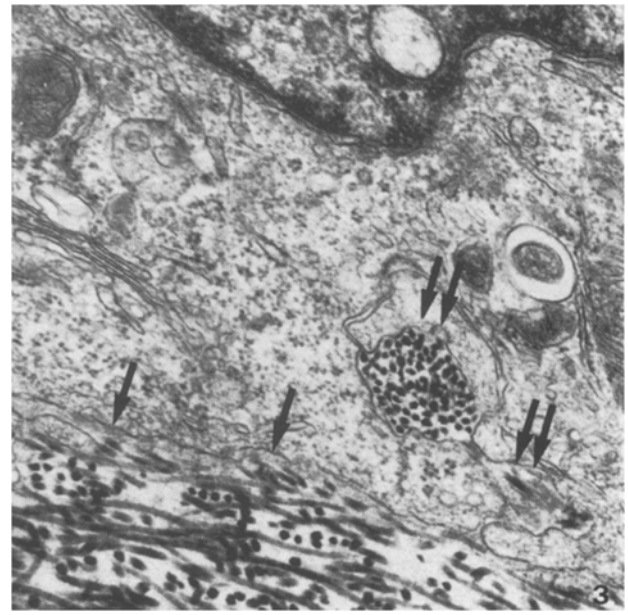

Fig. 3. Part of V2 carcinoma cell abutting upon extracellular matrix. Nucleus of carcinoma cell at top, cytoplasmic border of carcinoma cell indicated by arrows. Some remnants of basal lamina along this border are faintly visible. Extracellular matrix with sections of collagen microfibrils at bottom. 2 areas of matrix (double arrows) are surrounded by plump extensions of the carcinoma cell. 48 h after inoculation. × 58,500.

appears that lymphocytes possess a specific mechanism that is based on some kind of interaction with mesothelial cells and results in the formation of basal lamina-bound passageways of the exact size of the traversing cells. Conceivably, this mode of cooperation with mesothelial or endothelial cells also enables lymphocytes to cross tissue barriers in vivo. Further studies with the yolk sac model may contribute to a better understanding of the dynamic interaction of migrating cells and the extracellular matrix.

1 M.-F. Maignan, Biol. cell., in press.
2 G. Haemmerli and H. Felix, Leukemia Res. *1*, 79 (1977).
3 G. Haemmerli, H. Felix and P. Sträuli, Virchows Arch. B, Cell Path. *20*, 143 (1976).
4 H. Felix, G. Haemmerli and P. Sträuli, in: Dynamic Morphology of Leukemia Cells, p. 8. Springer-Verlag, Berlin/Heidelberg/New York (1978).
5 G. Haemmerli and P. Sträuli, Virchows Arch. B, Cell Path. *29*, 167 (1978).
6 S. Wood, Jr, Arch. Path. *66*, 550 (1958).
7 F.S. Steven and S. Itzhaki, Biochim. biophys. Acta *496*, 241 (1977).
8 M.K. Dabbous, A.N. Roberts and B. Brinkley, Cancer Res. *37*, 3537 (1977).
9 C. Biswas, W.P. Moran, K.J. Bloch and J. Gross, Biochem. biophys. Res. Commun. *80*, 33 (1978).

Sarcomere shortening and tension development during 'isometric' tetanus of muscle[1]

J.A. Barden and P. Mason

Muscle Research Unit, Department of Anatomy, The University of Sydney, Sydney (N.S.W. 2006) and School of Mathematics and Physics, Macquarie University, North Ryde (N.S.W. 2113, Australia), 19 March 1979

Summary. Laser diffraction and tension measurements from frog muscle during isometric tetanus reveal that the sarcomeres contract more rapidly than tension develops.

During muscle activation sarcomeres contract in response to the cycles of attachment, force-generation and detachment of crossbridges unless the muscle is kept strictly isometric[2]; this is only possible by the use of a servo-system such as the spot-follower[3]. In a nominally isometric experiment the sarcomeres may contract by as much as 5%, depending upon the compliance of the end-tissues and the mountings, until the tetanic level of tension is established. We have used an optical technique to measure the changes in sarcomere length of a frog sartorius muscle throughout the development of tetanus and also in the subsequent relaxation. By taking measurements at successive points along its length we obtained an average sarcomere contraction for the whole muscle and compared this with the corresponding development of tension.

Methods. The essentials of the experimental system have been outlined elsewhere[4,5]. An He-Ne laser is directed normally on a muscle specimen and the angular spacing of the first-order beams is sampled at 420 µsec intervals by chopping them with a rotating slotted disk. The sarcomere length at any instant is calculated from a knowledge of the system geometry and the time interval between the outputs of 2 photodiodes on which the 2 diffracted beams fall. Systematic noise is removed using a Hewlett Packard 2100S computer which also provides digital data every 420 µsec. Successive experiments were carried out, traversing the muscle length in 1 mm steps (approximately the diameter of the laser beam) in order to obtain sarcomere length records from all regions of the specimen. Each region provided a digital data file that was used to produce a summed and averaged data file equal to the total length change of all sarcomeres in the muscle occurring in response to the applied supramaximal stimulus. Tension was recorded using a Harvard 363 transducer.

Results. The summed and averaged response of sarcomeres from the full length of a frog sartorius is shown in the figure together with the tension record. The stimulus pulses commenced 100 msec after the computer began collecting diffraction data for noise reduction purposes. On the plateau of the sarcomere length record no sarcomere oscillation can be seen within a resolution of 2 nm, i.e. if periodic oscillations were present, their amplitude was less than 0.1%.

The figure also shows that the sarcomere length change procedes more rapidly than the development of tension. For instance the half-maximum of contraction is reached approximately 16 msec ($\Delta t_{1/2}$) before the half-maximum of tension. There is an even greater difference between the time-course of force and contraction following the cessation of stimulation. The sarcomeres expand much more slowly than the rapid fall in tension, reaching their half-maximum value some 200 msec after the tension. The sarcomere length in this 24 mm long muscle was 2.2 µm at rest, whilst the tension in full tetanus was 0.36 N. The temperature was controlled at 5 ± 0.25 °C.

Discussion. The variations in slope of the sarcomere shortening curve in the figure show that the sarcomeres start to contract at about the same time as tension starts to develop. By about 20 msec after the initial stimulus they reach their maximum rate of contraction ($250 \pm 50\%$ sec^{-1}) which remains constant for approximately a further 20 msec. This rate is substantially the same as V_{max}, the maximum velocity that can be generated when a frog muscle at this temperature contracts against zero load[5].

At the end of this period of maximum contraction velocity the tension has reached only about 20% of its full tetanic

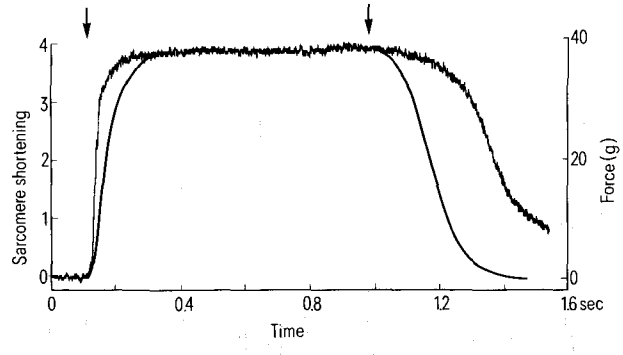

Average sarcomere shortening and tension developed in frog sartorius muscle throughout tetanus at 5 °C. Length and force scales have been chosen to assist in making comparisons. Arrows indicate the beginning and the end of the stimulating train of 40 V 200 µsec pulses.